REPORT DOCUMENTATION PAGE

Form Approved
OMB NO. 0704-0188

1. AGENCY USE ONLY (Leave Blank)	2. REPORT DATE	3. REPORT TYPE AND DATES COVERED
	8/9/2004	Final Report 3/1/01-5/31/04

4. TITLE AND SUBTITLE
Investigation of Quantum Dot Lasers

5. FUNDING NUMBERS
DAAD19-01-1-0331

6. AUTHOR(S)
Pallab Bhattacharya

7. PERFORMING ORGANIZATION NAME(S) AND ADDRESS(ES)
Solid State Electronics Laboratory
Department of Electrical Engineering and Computer Science
University of Michigan
Ann Arbor, MI 48109-2122

8. PERFORMING ORGANIZATION REPORT NUMBER

9. SPONSORING / MONITORING AGENCY NAME(S) AND ADDRESS(ES)
U. S. Army Research Office
ATTN: AMSRL-R0-S (TR)
P.O. Box 12211
Research Triangle Park, NC 27709-2211

10. SPONSORING / MONITORING AGENCY REPORT NUMBER
41272.9-EL

11. SUPPLEMENTARY NOTES
The views, opinions and/or findings contained in this report are those of the author(s) and should not be construed as an official Department of the Army position, policy or decision, unless so designated by other documentation.

12 a. DISTRIBUTION / AVAILABILITY STATEMENT
Approved for public release; distribution unlimited.

12 b. DISTRIBUTION CODE

13. ABSTRACT (Maximum 200 words)

Since the first demonstration of room-temperature operation of self-assembled quantum dot (QD) lasers about a decade ago, there have been great strides in improving the characteristics of these lasers and their performance currently match or surpass those of quantum well lasers. There are, however, unique problems that limit the performance of conventional separate confinement heterostructure (SCH) QD lasers, compared to what is expected from "ideal" lasers with near singular density of states. In the study reported here, unique insights and solutions to these problems have been demonstrated and reliable quantum dot lasers, that surpass quantum well lasers in performance characteristics, have been demonstrated. The characteristics of distributed feedback (DFB) quantum dot lasers have been studied and are described. By utilizing the concepts of tunnel injection and p-doping 1.0μm and 1.3μm quantum dot lasers with high differential gain, $T_0 = \infty$, modulation bandwidth ~25GHz, a-factor less than unity and zero chirp have been achieved. This final report describes the properties of these unique devices.

14. SUBJECT TERMS			15. NUMBER OF PAGES
			16. PRICE CODE
17. SECURITY CLASSIFICATION OR REPORT	18. SECURITY CLASSIFICATION ON THIS PAGE	19. SECURITY CLASSIFICATION OF ABSTRACT	20. LIMITATION OF ABSTRACT
UNCLASSIFIED	**UNCLASSIFIED**	**UNCLASSIFIED**	**UL**

Final Report

1. Title of Project: "Investigation of Quantum Dot Lasers"

2. Grant Number: DAAD 19-01—1-0331

3. Period Covered by Report: 03/01/01-05/31/04

4. Name of Institution: University of Michigan

5. Principal Investigator: Pallab Bhattacharya

6. Scientific Progress and Accomplishments:

• Introduction

Since the first demonstration of room-temperature operation of self-assembled quantum-dot (QD) lasers about a decade ago, there have been great strides in improving the characteristics of these lasers and their performance currently match or surpass those of quantum well lasers. There are, however, unique problems that limit the performance of conventional separate confinement heterostructure (SCH) QD lasers, compared to what is expected from "ideal" QD lasers with near singular density of states. The rather wide inhomogeneous broadening in QDs broadens their gain spectrum considerably from the ideal delta-function spectrum. The frequency-selective feedback mechanism in distributed feedback (DFB) lasers is traditionally an appealing method for sharp single-mode operation of lasers. Thus, using DFB mirrors is a reasonable approach to improve the gain spectrum of QD lasers. Also, the peak of the gain spectrum in quantum well (QW) lasers is largely temperature-dependent, which degrades the performance of the devices. This effect appears to be much less severe in QD-based lasers, which has been another motivation for the present work on QD DFB lasers.

Furthermore, SCH QD lasers suffer from significant hot-carrier effects and associated gain compression due to the large density of states of the wetting layer and barrier states, compared with that in the quantum dots. As a result, the conventional devices cannot be typically modulated at bandwidths above 6-7 GHz. Also, due to small energy spacing in the valence band, hole distribution is thermally broadened into the many available states and large injected hole density is required for a large gain in the ground state and electron density is also increased according to charge neutrality. Thus, the characteristics temperature, T_0, is also rather low in SCH QD lasers.

Two solutions have been proposed to circumvent the inherent unique problems of conventional SCH QD lasers, namely, tunneling injection (TI) and p-doping of the dots. In the tunnel injection scheme, "cold carriers" are injected directly into the ground state of the QDs by phonon-assisted tunneling from an injector layer and are removed by stimulated emission at approximately the same rate. Therefore, the differential gain of the lasers can be optimized and hot carrier effects are minimized. In the p-doping scheme, extra holes are provided at the ground state energy by either direct doping of the dots or by modulation doping of the GaAs barriers. These extra holes ensure population inversion with less injected holes from the contacts, and consequently the electron population in the dots and their leakage

into barrier and waveguide layers is reduced as well. Large values of T_0 are expected in p-doped QD lasers.

This final report summarizes the successful design, fabrication and characterization of high performance 1.0μm QD-DFB lasers, 1.0μm QD-tunnel injection lasers (undoped and p-doped) and 1.3μm p-doped QD lasers. As will be evident, we have demonstrated record performance of these unique devices in terms of differential gain, modulation bandwidth, temperature dependence, chirp and linewidth enhancement factor.

- **Accomplishments**

- **Quantum Dot Distributed Feedback Lasers**

The inhomogeneous broadening of the photoluminescence and gain spectra in quantum dots, due to the random variation in their size, typically makes the output spectrum of Fabry-Perot QD lasers multi-mode and unstable. The distributed feedback (DFB) scheme is a well-known technique to obtain narrow linewidth single-mode lasers. Gain-coupled with external gratings have been used to avoid regrowth.

Figure 1(a) shows the QD laser heterostructure consisting of 4 coupled layers of $In_{0.40}Ga_{0.60}As$ QDs buried in a GaAs guide layer and surrounded by 1.0μm $Al_{0.30}Ga_{0.70}As$ claddings. The heterostructure was grown by solid source molecular beam epitaxy (MBE) on (001) n-GaAs substrate. The quantum dots were grown at 520°C and the GaAs and AlGaAs layers were grown at 620 and 650°C, respectively. After depositing 3.0μm wide p-metal contacts, a combination of self-aligned dry and wet etching techniques were used to define mesas from approximately 0.2 μm above the active region. The etch depth was optimized to achieve the desired coupling coefficient and optical loss in the metal grating, to be subsequently formed. Electron beam lithography was used to define the metal grating with 0.3 μm period and 50% duty cycle, in order to obtain a lasing wavelength of 1.0 μm. Due to the non-planar surface of the e-beam sample, high electron energies are required to ensure the extension of the lateral grating to the edge of the mesa. A 100 keV Leica VB6 electron beam system with 1 nA beam current was used to expose and define the grating pattern on 150 nm e-beam resist. 45 nm of chromium was next evaporated and lifted off to create the metal grating. Figure 1(b) shows a surface-electron microscopy image of a section of the metal grating and ridge. 1mm long DFB lasers were fabricated by standard processing.

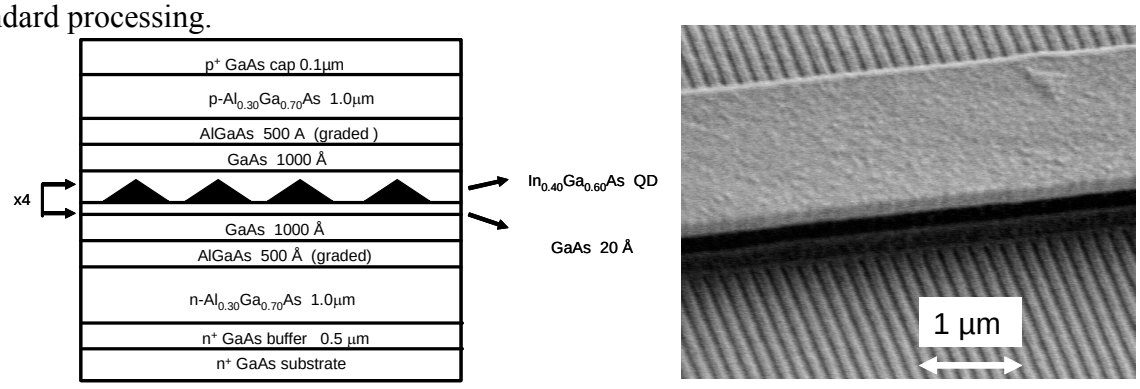

(a) (b)

Figure 1: (a) Schematic of $In_{0.40}Ga_{0.60}As$/GaAs quantum dot distributed feedback laser heterostructure grown by molecular beam epitaxy, and (b) scanning electron microscopy image of a section of the Cr grating and the waveguide ridge.

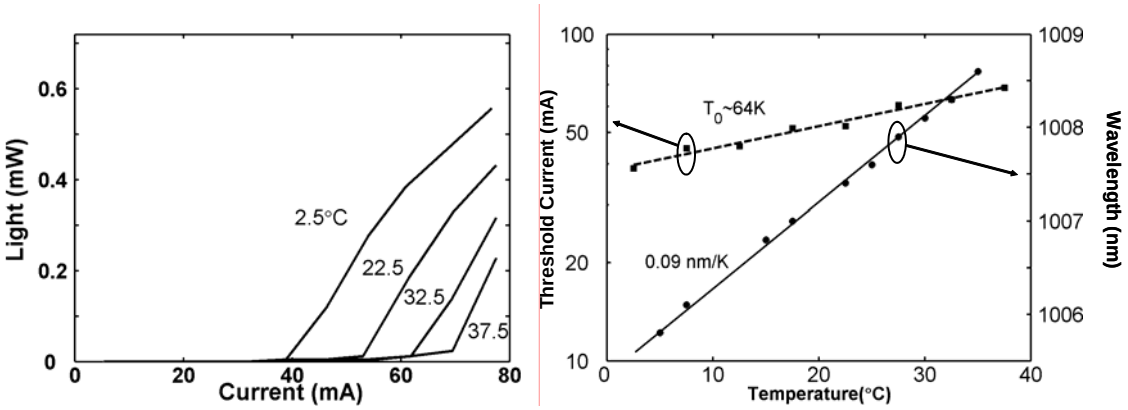

Figure 2: (a) The temperature-dependent light current characteristics; (b) Measured temperature dependence of the threshold current (squares) and lasing wavelength (circles) of InGaAs/GaAs QD DFB. lasers. The dashed and solid lines are fitted to the data

Light-current (LI) characteristics of the QD DFB lasers were measured under pulsed bias conditions. At room temperature, the threshold current is 60 mA and the differential quantum efficiency is ~0.1W/A. The temperature dependence of the threshold current and the peak wavelength of the output spectrum were also measured. From the data shown in Fig. 2, the characteristics temperature, T_0, derived to be 64 K around room temperature and the wavelength is found to shift linearly with a slope of 0.09nm/K. In comparison, this shift is typically >0.25nm/K for a Fabry-Perot QD laser. Figure 3 depicts the room-temperature output spectrum of the laser at $1.2I_{th}$, measured with a HP 70952B optical spectrum analyzer. The side-mode suppression ratio is 30dB and the linewidth (full-width at half maximum) is 4Å.

The modulation response for the lasers at room-temperature and at different injection currents is shown in Fig. 4(a). The maximum 3-dB bandwidth, measured for an injection bias of 78 mA is ~5 GHz. The measured bandwidth is similar to what has been recorded for separate confinement heterostructure (SCH) Fabry-Perot ridge waveguide QD lasers. We also measured the chirp in the DFB lasers during direct modulation at room temperature by measuring the broadening of a single longitudinal mode using an optical spectrum analyzer with a resolution of 0.8 Å. The sinusoidal modulation current was superimposed on a pulsed d.c. bias current. The dc bias is 82 mA, the peak-to-peak modulation current has varied from 0 to ~40 mA and the modulation frequency was varied upto 2 GHz. The measured data are shown in Fig. 4(b). No measurable chirp was observed in these devices even under large signal modulation conditions. The chirp in a semiconductor laser is directly proportional to the linewidth enhancement factor, α, which has been measured to be extremely low and <1 in QD lasers, as follows.

A theoretical analysis of the threshold current density of QD-DFB lasers was conducted. The gain of the QD active region can be calculated from

$$g(\hbar\omega) \propto \frac{1}{\hbar\omega V_{dot}} \sum_{i,j} \left| \varepsilon . P_{ij} \right|^2 G(\hbar\omega, E_{ij}, \sigma_{gain})(f_n(E_i^e) - f_p(E_j^h))$$

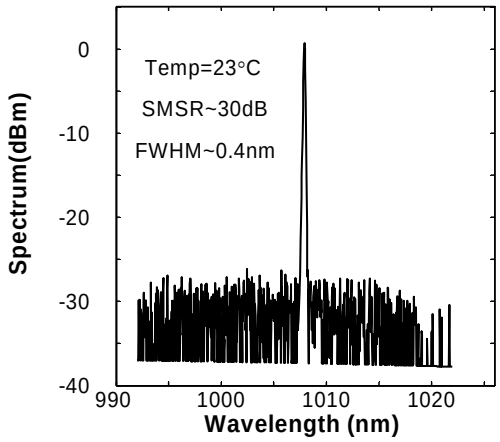

Figure 3: The output spectrum of the InGaAs/GaAs QD DFB lasers at room temperature.

, where a 20 meV Gaussian inhomogeneous broadening is assumed to be dominant on the dot density of states. The optical matrix element P_{ij} can be calculated from electron-hole wavefunctions. The wavefunctions are calculated by 8x8 *k.p* model simulator after obtaining the strain profile in the dot from valence-force field model. The calculated *g* for various *e-h* pair injections into one dot is shown in Fig. 5(a).

Three different spontaneous emission components were assumed to contribute to the current density, i.e., the quantum dots, the wetting layer (assumed to be a well) and the bulk matrix GaAs:

$$R_{sp}^{i}(\hbar\omega) \propto \frac{1}{\hbar\omega} |P_{ave}^{i}|^2 \rho_{red}^{i}(\hbar\omega, E^{i}) \rho_{opt}(\hbar\omega) f_e (1 - f_v)$$

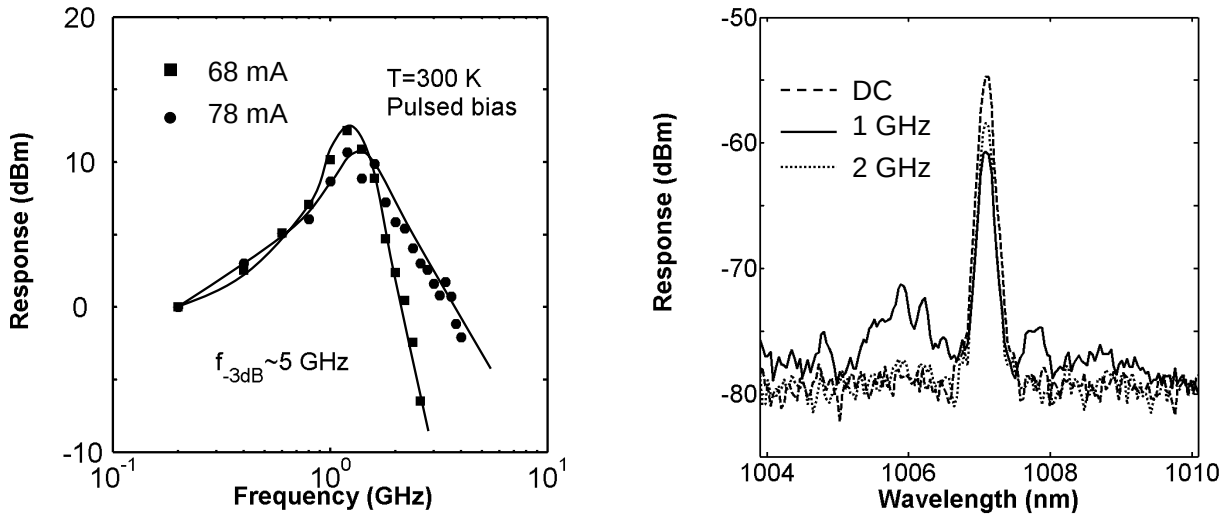

(a) (b)

Figure 4: (a) Modulation frequency response of quantum dot DFB laser at different injection currents. Curves are guides to the eye; (b) optical spectrum of the DFB lasers at 82 mA d.c. bias and 40 mA a.c. signal for 1 and 2 GHz modulation frequencies.

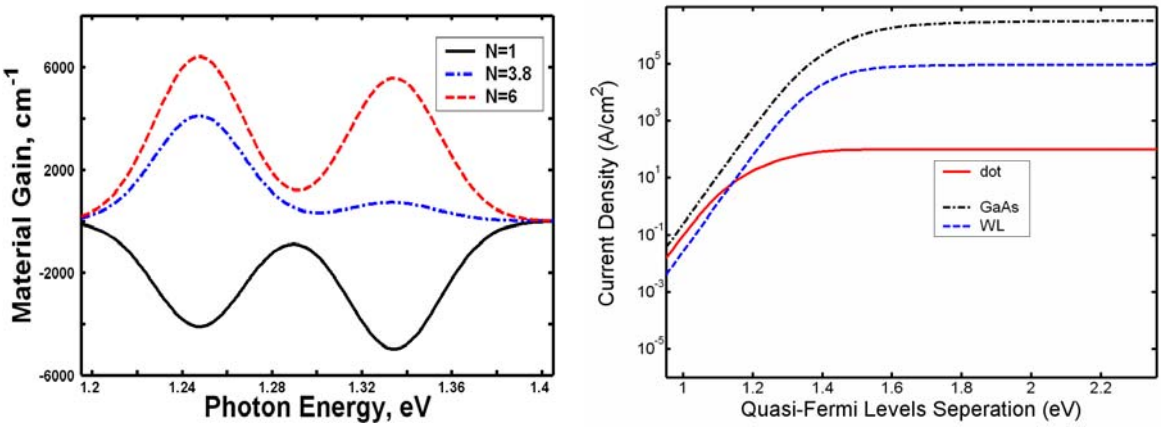

(a) (b)

Figure 5: (a) Gain vs. photon energy for different *e-h* pair injections into a QD; (b) Different components of current density vs. bias in a QD-DFB laser.

The corresponding current densities are plotted in Fig. 5(b). Threshold modal gain in the DFB structure can be calculated by operational matrix method and the predicted threshold current density of QD-DFB lasers is about 900 A/cm^2, i.e., 48mA in our structure, which is close to the measured 55mA.

In conclusion, gain-coupled quantum dot distributed feedback lasers with chromium lateral grating were fabricated and characterized. The lasers exhibit stable single-mode operation at 1006 nm with 30 dB side-mode suppression ratio and linewidth of 4Å at room-temperature. The lasers have 3dB modulation bandwidth of 5 GHz. Frequency chirp was not observed in the devices even for large-signal modulation conditions.

• Quantum Dot Tunnel Injection Lasers

To achieve large modulation bandwidths in semiconductor lasers, the photon density in the cavity and the injected carrier density have to be large. In a conventional separate confinement heterostructure (SCH) device, while injected carriers lose energy and fill the lasing states, carrier heating simultaneously forces them out towards higher energies and causes leakage to adjoining layers. In quantum dot (QD) lasers, these problems can become worse due to the "hot carrier" effects, which have been studied by us in detail by two- and three-pulse pump-probe differential transmission spectroscopy. On the other hand, if electrons are introduced directly into the lasing states by phonon-assisted tunneling and the tunneling rate is comparable to the stimulated emission rate, the carrier distribution in the active region will remain "cold" and hot-carrier effects are minimized. It is important to note that the hole relaxation rates in QDs and other quantum confined structures are very large due to the multiplicity of the levels, band mixing and efficient hole-phonon coupling.

The QD laser heterostructure was grown by molecular beam epitaxy (MBE) and the conduction band profile is illustrated in Fig. 6(a). The 95Å $In_{0.25}Ga_{0.75}As$ injector well is grown at 490ºC, the three coupled QD layers are grown at 525ºC and the rest of the structure is grown at 620ºC. The samples exhibit luminescence peaks at 1.26 eV and 1.3 eV from the QDs and from the $In_{0.25}Ga_{0.75}As$ quantum well injector, respectively. The wavelength of the dot luminescence peak is controlled by adjusting the

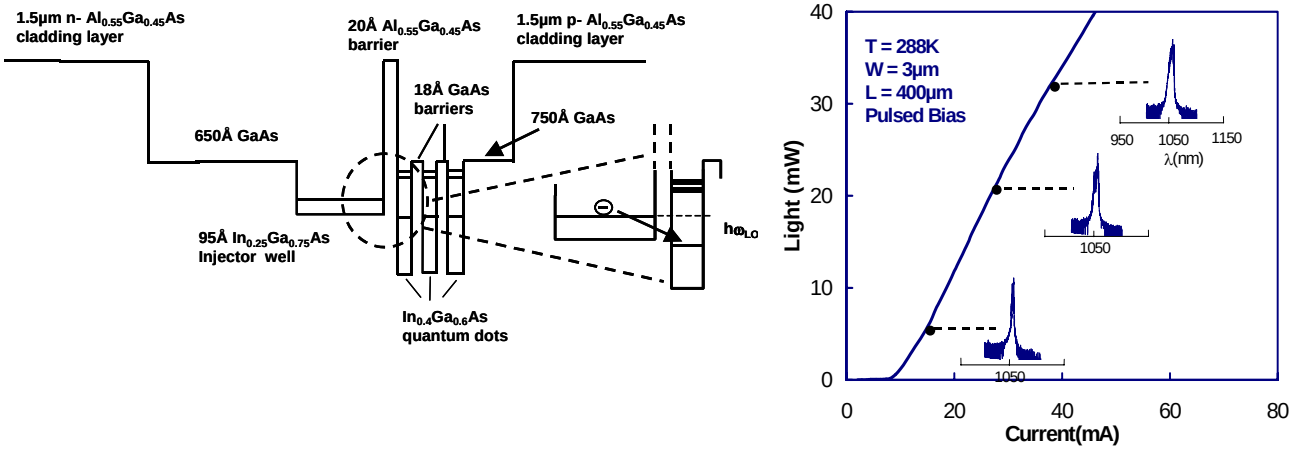

(a) (b)

Figure 6: (a). Conduction band profile of the tunnel injection quantum dot laser heterostructure under flat-band The conditions; (b) measured light-current characteristics of a single-mode tunnel injection quantum dot laser. insets depict the spectral outputs at various currents.

InGaAs dot charge during epitaxy. The energy separation, in the conduction band, between the injector well states and the QD ground states is ~ 36 meV at room temperature. This energy separation ensures *LO phonon-assisted tunneling* from the injector well to the dot ground states through the 20Å $Al_{0.55}Ga_{0.45}As$ barrier layer. An interesting observation was made in that the photoluminescence linewidth for the ground state quantum dot transition in the tunneling injection structures was always quite small. The linewidth (23meV at 20K) is almost a factor 2-3 lower than that measured in conventional coupled quantum dot heterostructures. We believe that the *phonon-assisted* tunneling process helps to *select* the dots contributing to the lasing process and this filtering adds to the homogeneity of the dot sizes.

Ridge waveguide lasers 3μm×400μm long were fabricated by standard lithography, wet and dry etching, and metallization techniques. The cleaved facets were left uncoated. The threshold current of the device with continuous-wave (CW) biasing is 12mA at room temperature. The measured light-current characteristics under pulsed biasing condition (1μs with 1% duty cycle) are shown in Fig. 6(b). High values of slope efficiency (0.86W/A) and differential quantum efficiency ($\eta_d = 0.73$) are measured in these devices. From measurements on lasers with varying cavity lengths, an internal quantum efficiency $\eta_i = 0.85$ and cavity loss coefficient $\gamma = 8.2 cm^{-1}$ are derived. The lasing peak wavelength under threshold conditions is recorded at 1.069μm (1.16eV).

The temperature-dependent light-current characteristics of a 400μm long device, measured under the pulsed conditions. The light output is measured from a single uncoated facet. From the two distinct slopes indicated by the continuous lines, values of $T_0 = 363K$ for 5ºC < T < 60ºC and $T_0 = 202K$ for 60ºC < T < 100ºC are derived. These are the highest values of T_0 measured in these temperature ranges in undoped quantum dot lasers. The high device efficiencies and the high values of T_0 indicate minimization of carrier leakage from the gain region and parasitic recombination in optical confinement layers.

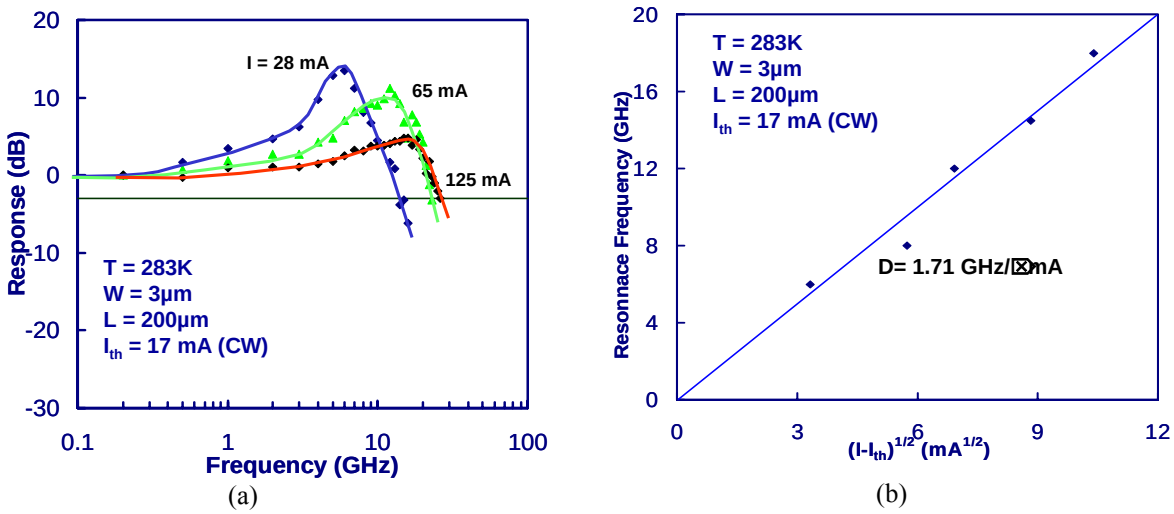

(a) (b)

Figure 7: (a) The small-signal modulation response with varying injection currents at 283K; (b) plot for the variation resonance frequency versus the square root of injected current.

The small-signal frequency response of the 200μm tunnel injection QD laser for varying injection currents is shown in Fig. 7(a). The continuous lines are guides to the eye. Shown, as insets in Fig. 7(b) are the spectral outputs at these injection currents, which confirm that lasing from the ground state is maintained. A bandwidth of f_{3dB} = 23GHz is measured for I ~ 125mA.The modulation response shows a gain compression limited behavior and analysis of the modulation data gives us a gain compression factor, $\varepsilon = 8\text{x}10^{-16}$ cm^3. This value is a factor of 50 smaller than those measured in the best SCH quantum dot lasers. The modulation efficiency, which is the slope of the plot of the resonance frequency f_r of the modulation response as a function of the square root of the output power (as shown in Fig. 7(b)), is ~ 1.7GHz/$mW^{1/2}$. From this value of the modulation efficiency and using a dot fill factor of ~ 28% and a confinement factor Γ~$2.5\text{x}10^{-3}$, we derive the value of differential gain, dg/dn ~ $3\text{x}10^{-14}$ cm^2 at room temperature. This value of differential gain is higher than those measured in separate confinement heterostructure QD lasers grown under identical conditions.

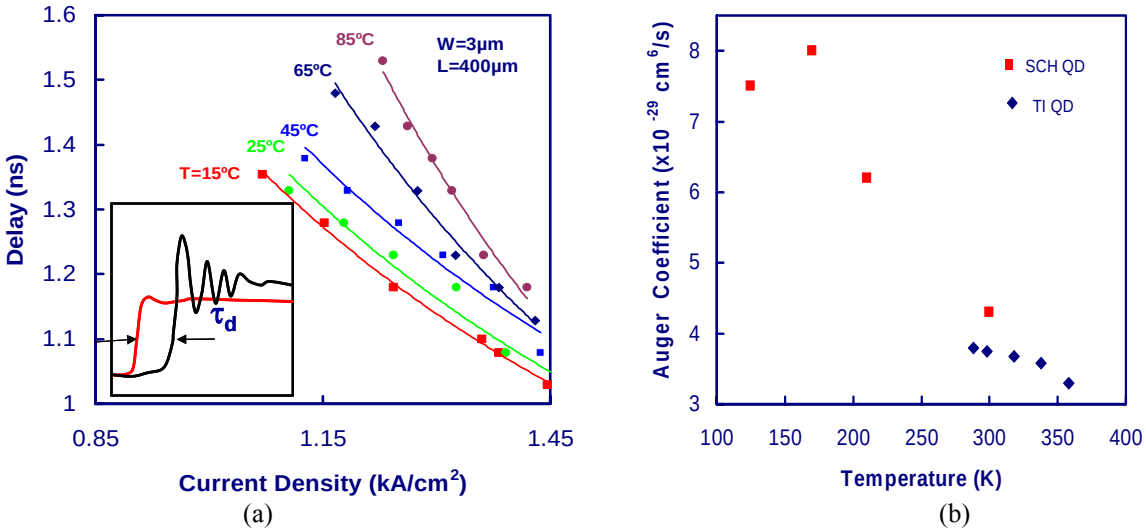

(a) (b)

Figure 8: (a). Measured delay times in TI QD laser as a function of injected current density at different ambient temperatures; (b) auger recombination coefficients as a function of temperature in both SCH and TI QD lasers.

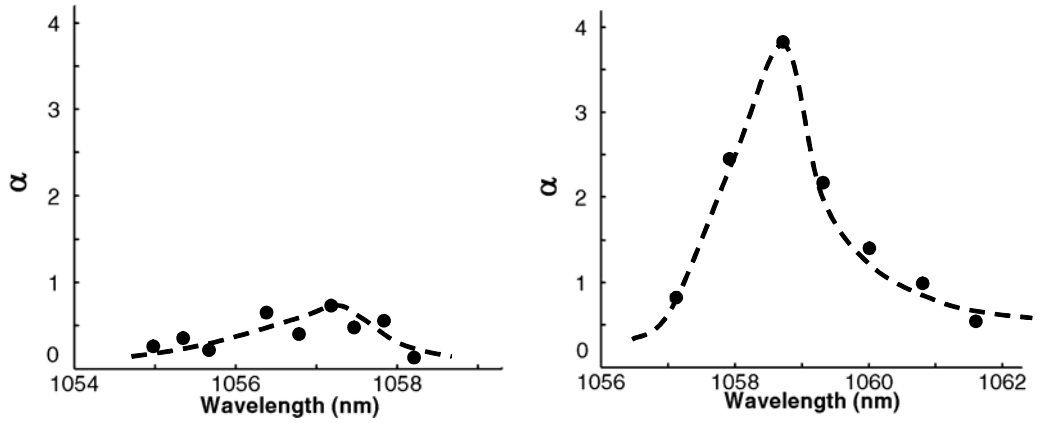

(a) (b)

Figure 9: Measured linewidth enhancement factor at subthreshold peak wavelengths of (a) tunnel injection quantum dot laser, and (b) SCH quantum well laser. The dashed lines are guides to the eye.

The large-signal modulation measurements were made on the 400μm long single-mode ridge waveguide TI lasers at different temperatures. The lasers are pulse biased with a 10% duty cycle from I = 0 to I(>I_{th}) with a 100ps (20%-80%) rise time electrical pulses. The output is detected with an InGaAs photoreceiver. The delay time between the electrical and optical signal is measured with a high-speed digital sampling oscilloscope, taking into account the delays due to optical fiber, RF cables and the photoreceiver. The delay times are measured between the 50% points in the applied electrical pulse and the output optical signal. Figure 8(a) shows the experimentally determined turn-on delay times as a function of bias current density at different ambient temperatures. The increase in the bias current density decreases the recombination lifetime and consequently the delay time.

To match the experimental and theoretical threshold current densities at each temperature, the inhomogeneous broadening in the quantum dots is varied. The Auger coefficient is obtained by minimizing the root mean square error between the theoretical and experimental delay times. The variation of Auger coefficient C_a with temperature in a tunnel injection QD laser is shown in Fig. 8(b). For comparison purposes, the measured coefficients in a SCH-QD laser are also shown. The reduced Auger coefficients in TI quantum dot lasers reflects a smaller hot carrier density.

Spatial coherence and lateral mode control of the output beam of semiconductor lasers at high power operation are important specifications for practical applications. At high levels of carrier injection, filamentation occurs due to increase of refractive index and self-focusing of the optical mode in the gain medium. The degree of filamentation is strongly dependent on the linewidth enhancement factor, α, which itself is inversely proportional to the differential gain. Large differential gains have been demonstrated in QD lasers and low α-factors have also been reported. It is therefore expected that filamentation will be greatly reduced and such reduction has been demonstrated in broad area and narrow stripe InGaAs QD lasers. Here, we report very low values of α-factor and associated suppression of filamentation in single-mode, ridge waveguide $In_{0.4}Ga_{0.6}As$/GaAs self-assembled TI QD lasers at room temperature. The results have been compared with those from conventional SCH quantum well (QW) lasers. The heterostructure, growth and processing of the TI lasers were given in previous reports.

The threshold currents for 400μm long devices are 16 and 10mA for the TI-QD and QW lasers, respectively. The lasing wavelengths at threshold are 1056.8 and 1059.4nm for the TI-QD and QW lasers, respectively. The linewidth enhancement factors of the two types of lasers were measured from the net modal sub-threshold spectrum. The sub-threshold spectra were measured with a HP 70952B optical spectrum analyzer under pulsed bias. The measured linewidth enhancement factors are plotted against the peak wavelength of the subthreshold spectrum for the TI-QD and QW lasers in Figs. 9(a) and (b), respectively. The QW laser exhibits a value of $\alpha \cong 3.7$ at lasing wavelength. In the tunnel injection QD laser, $\alpha \cong 0.73$ at the lasing wavelength and is as small as 0.1 at other wavelengths. These are amongst the smallest values of α-factor measured in any semiconductor laser. The low α-factor measured in our tunnel injection lasers is a reflection of the fact that the large differential gain and symmetric gain spectrum in quantum dots, together with minimization of carrier leakage, play important roles.

To further study the effect of reduction in α, the near-field pattern was measured as a function of injection current in 400 μm TI-QD and 800 μm QW lasers. Examples of the spatial intensity through the center of the junction plane for different bias levels are shown in Figs. 10(a) and (b) for the TI-QD and QW lasers, respectively. The insets are the two-dimensional beam pattern at the corresponding highest shown biases. The QW laser remains single-mode upto an injection current of $1.87I_{th}$, but clearly suffers from filamentation above that and two distinct lobes are observed at higher biases. Such filamentation were previously reported in narrow ridge waveguide QW lasers. In contrast, filamentation is not evident in the intensity distribution of the TI-QD laser and the near-field pattern maintains a Gaussian form upto a bias of $\sim 3.5I_{th}$.

Since chirp is directly proportional to α, TI-QD lasers are expected to have low chirp. We measured the chirp in these devices and compared it with QW lasers. The envelope of the dynamic shift in wavelength of the sinusoidal modulation signal was recorded with the HP 70952B optical spectrum analyzer and a resolution of 0.8Å. The evaluated chirp for TI-QD and QW lasers versus peak-to-peak

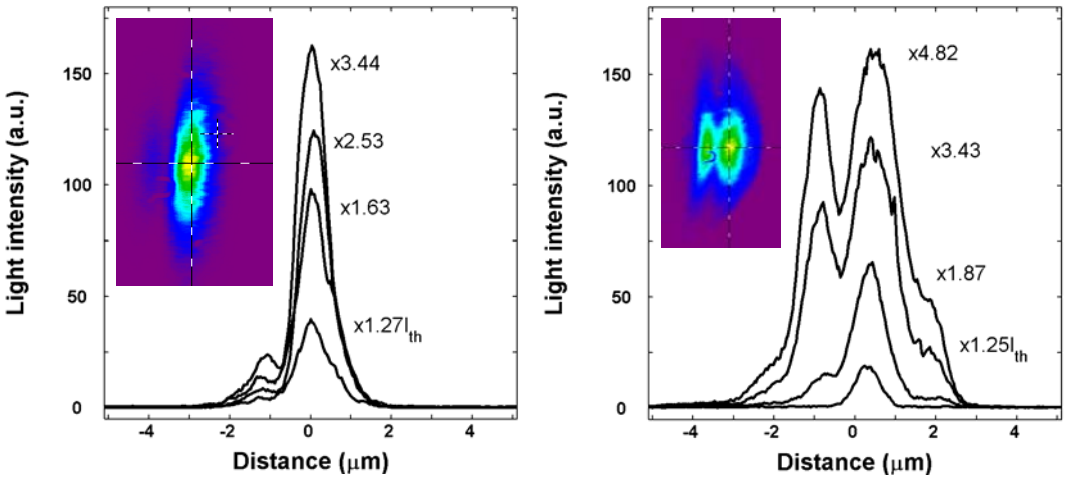

Figure 10: Spatial intensity distribution of near-field mode pattern along junction plane at cleaved edge fro different biases for (a) tunnel injection quantum dot laser, and (b) SCH quantum well laser. The distances are measured from the center of ridge. Insets show the near field images of the modes at the highest biases.

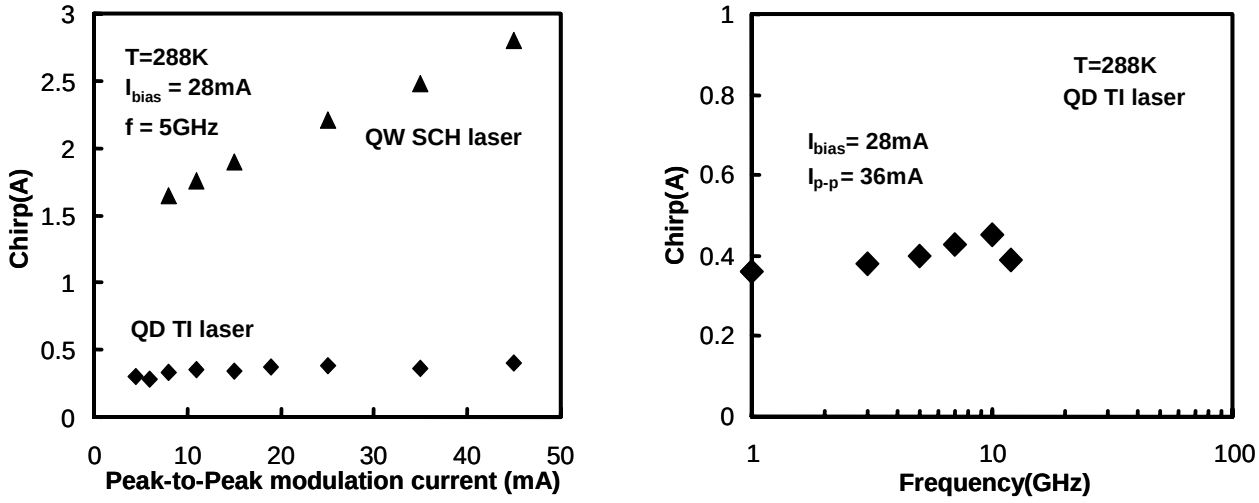

(a) (b)

Figure 11: (a) Measured chirp for tunnel injection quantum dot laser and SCH quantum well laser at different peak-to-peak modulation currents; (b) Chirp versus frequencies in tunnel injection quantum dot lasers.

modulation current are shown in Fig. 11(a) at the modulation frequency of 5 GHz and a dc bias of 28 mA. The chirp of the QW lasers varies between 1.6 and 2.9 Å and is comparable to previously reported values. Figure 11(b) shows the chirp on the TI-QD lasers versus frequency at a constant ac bias of 36 mA. As expected, TI-QD lasers show much lower chirp of <0.6 Å at different ac biases and even at high frequencies.

In conclusion, we demonstrate enhanced steady state and dynamic characteristics in tunnel injection QD lasers by utilizing *phonon assisted tunneling*.

- **p-Doped Quantum Dot Lasers**

We have studied the impact of p-doping on (a) conventional 1.3µm SCH quantum dot lasers; and (b) 1.0µm tunnel injection quantum dot lasers. We demonstrate 1.3µm p-doped QD SCH lasers with zero temperature dependence of the threshold current (T_0=∞) and the output slope efficiency from 5-75°C. High modulation bandwidths comparable to quantum well lasers (25GHz) are reported in 1.0µm p-doped tunnel injection QD lasers, which is higher than our previous results on undoped TI QD lasers. We also report negligible linewidth enhancement factor (α~0), and ultra-low chirp (<0.4Å) in these devices.

(a) 1.3µm p-Doped Quantum Dot SCH Lasers

The schematic of the 1.3µm InAs quantum dot SCH lasers, grown by MBE, is shown in Fig. 12. Both undoped and p-doped QD lasers were grown and fabricated. In the doped lasers, the modulation doping of the dots was achieved by delta-doping the GaAs barrier/waveguide regions separated from the neighboring quantum dot layer by 14nm. The doping concentration was varied to provide sheet acceptor concentration per quantum dot layer varying in the range (0-2)×10^{12} cm^{-2}. The optimum doping level

was determined by studying the luminescence of the dots and the device characteristics. Mesa-shaped broad area (100μm-wide) and single-mode ridge waveguide lasers (3-μm ridge width) were fabricated by standard lithography, wet and dry etching, and metallization techniques. 200-2000μm long lasers were obtained by cleaving. A dielectric distributed Bragg reflector mirror with 95% reflectivity was deposited on one facet of the 1.3μm QD lasers, while the other facet was left uncoated. Both cleaved facets were left uncoated in the 1.0μm tunnel injection p-doped QD lasers.

Light-current (LI) measurements were done, both in continuous wave (CW) and in pulsed mode (1μs, 10 kHz) of biasing, with the devices mounted on a heat-sink with stabilized temperature. From the LI characteristics of the broad area lasers of varying cavity length at 15°C, we determine the value of internal quantum efficiency, η_i, and cavity loss, γ, to be 62% and 6.6 cm^{-1}, respectively, for the p-doped samples with an optimized delta-doping of $5\times10^{11}cm^{-2}$. The value of J_{th} is 390A/cm^2 for 400μm cavity length. For the undoped QD lasers, η_i, γ, and J_{th} are 0.89, 4.3 cm^{-1}, respectively. The threshold current density is about 155 A/cm^{-2} for 400μm cavity length, which is less than the p-doped samples. The LI characteristics of a single mode p-doped laser, measured at various temperatures, are shown in Fig. 13(a). Plotted in Fig. 13(b) are the threshold current and differential efficiency as a function of temperature, as derived from the data of Fig. 13(a). It is evident that I_{th} is independent of temperature in the range 5-75°C ($T_0=\infty$) and so is the differential efficiency. Similar results were obtained under CW bias and for the broad area lasers. *This is the first time that a semiconductor laser has displayed such temperature invariant features.* In contrast, the conventional undoped QD lasers exhibit T_0=69K in the same temperature range. It is noteworthy that complete temperature independence is a property of "ideal" QD lasers with singular density of states. However, with self-organized dots $T_0=\infty$ is unattainable, since the emission and the density of states function of self-organized quantum dots are broadened inhomogeneously due to size fluctuations.

In order to understand these trends, we have analyzed the measured threshold current data by taking into account radiative recombination in the quantum dots, wetting layer, and GaAs barrier/waveguide regions, and Auger recombination in the dots. Non-radiative recombination in the wetting layer, GaAs

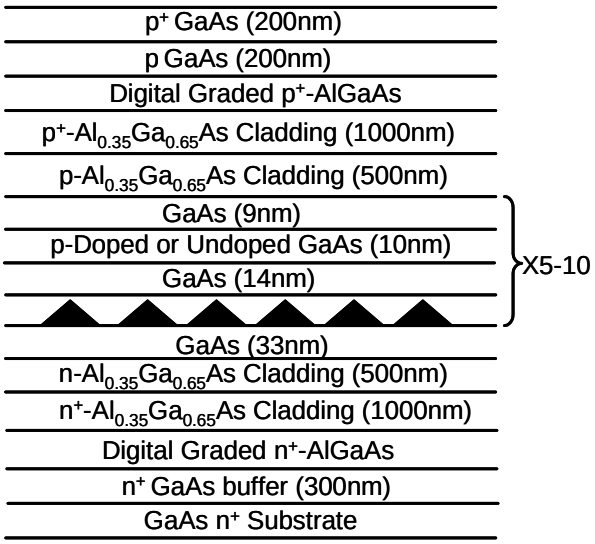

Figure 12: Heterostructure schematic of 1.3μm p-doped and undoped self-organized quantum dot lasers.

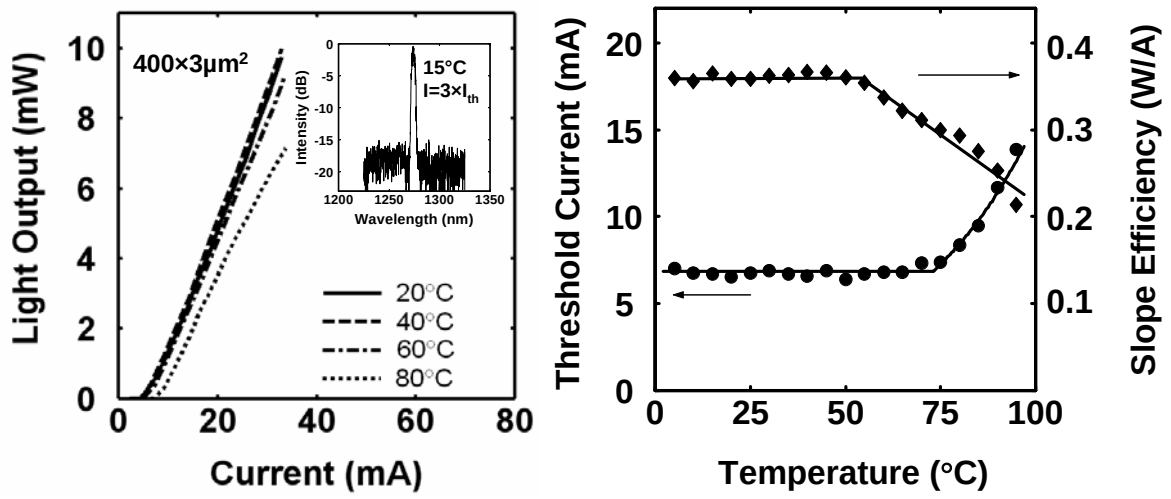

(a) (b)

Figure 13: (a) Pulsed light-current characteristics of 1.3μm p-doped single mode QD lasers at different temperatures. The inset shows the output spectrum at 15°C; (b) variation of threshold current and slope efficiency of the lasers with temperature. The lines are fits to the experimental data.

regions, and $Al_{0.35}Ga_{0.65}As$ outer cladding layers have been neglected. The modal gain in the devices was calculated by including interband transitions between the ground and first two excited states and by assuming inhomogeneously broadened Gaussian linewidth of 50meV for the transitions. The threshold condition and the measured values of cavity loss are used to determine the carrier densities in the different regions. A second harmonic oscillator model for 10 degenerate hole states with 10meV spacing was used. The temperature dependence of the bound states in the dots and the energy levels in the wetting layer and GaAs barrier regions were taken into account. Fermi-Dirac statistics was employed with the assumption of flat-band quasi-Fermi levels across the active region at threshold and complete ionization of dopants. In the case of the p-doped QD lasers, charge neutrality was assumed to exist between each QD layer and the immobile ionized dopants in the neighboring barrier.

The results of the analysis are depicted in Figs. 14(a) and (b) for p-doped and undoped lasers, respectively, together with the measured threshold current densities of single-mode devices. The temperature dependence of the different current components and their cumulative effect are shown. It is evident from Fig. 14(b) that radiative recombination in the quantum dots is the dominant factor contributing to the threshold current at temperatures below 330K in the undoped QD lasers. At higher temperatures, an exponential increase of recombination in the barriers increases the temperature dependence of the current. The value of T_0 is 79K, which is close to the measured value of 69K. On comparing the result of Figs. 14(a) and (b), it is also evident that the value of J_{QD}, resulting from radiative recombination in the dots, decreases upon p-doping. However, our experimental observation of an invariant J_{th} in the temperature range $5 \leq T \leq 75$°C (Fig. 3(a)) and an increase in the value of J_{th}, compared to the undoped QD lasers, can only be explained by considering Auger recombination. The increase of hole population in the quantum dots due to modulation doping causes an increase in the rate of Auger recombination, particularly at low temperatures. Upon incorporating the measured temperature dependence of Auger recombination in 1.0μm dots and using slightly different values of the coefficients

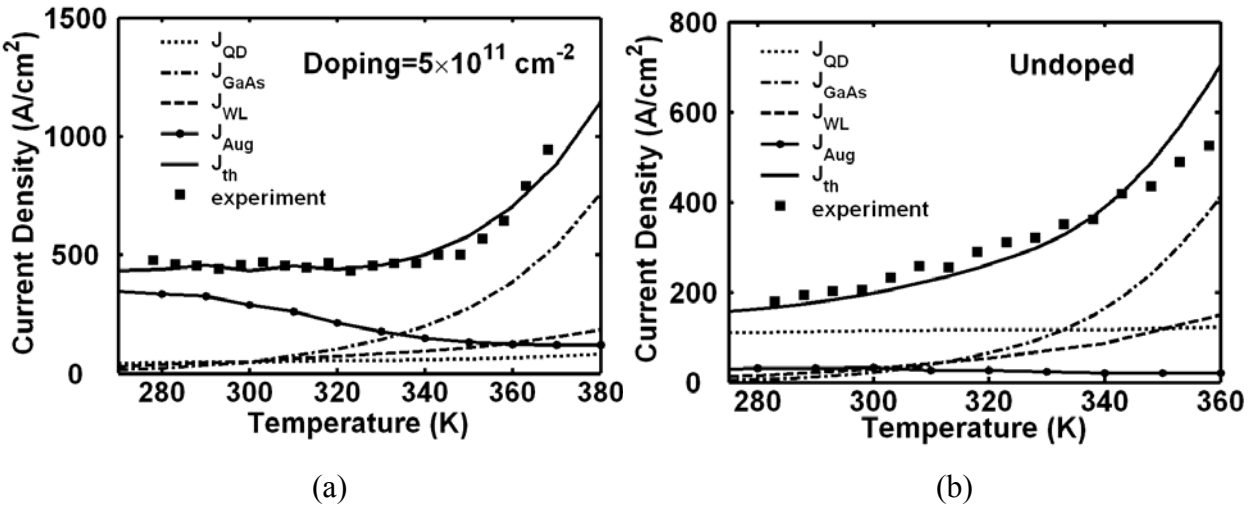

Figure 14: Variation of calculated and measured threshold current density, J_{th}, in (a) p-doped, and (b) undoped self-organized quantum dot lasers. Also shown are the contributing current components resulting from radiative recombination in the dots (J_{QD}), recombination in the barrier/waveguide regions (J_{GaAs}), wetting layer (J_{WL}), and Auger recombination in the dots (J_{Aug}).

for the present 1.3μm dots, the temperature invariant measured threshold current of Fig. 14(a) can be explained. The exponential increase of recombination in the barrier/waveguide regions with temperature is compensated by the decrease of Auger recombination in the same temperature range.

In conclusion, we have analyzed the measured temperature variation of the threshold current of undoped and p-doped self-organized 1.3μm quantum dot lasers. It is found that Auger recombination in the dots plays an important role in establishing temperature invariance of J_{th} in the range 5-75°C.

(b) 1.0μm p-Doped Tunnel Injection Quantum Dot Lasers

The heterostructure and conduction band profile of 1.0μm InGaAs tunnel injection QD lasers are similar to undoped samples, as schematically shown in Fig. 6(a). The wavelength of the dot luminescence peak is controlled by adjusting the InGaAs dot charge during epitaxy. The energy separation in the conduction band between the injector well states and the QD ground state is ~36 meV at room temperature. This energy separation ensures longitudinal optical (LO) phonon-assisted tunneling from the injector well to the dot ground states through the 35 Å $Al_{0.62}Ga_{0.38}As$ barrier layer. The p-doping is again provided by delta-doping ($5\times10^{11}cm^{-2}$) the GaAs barrier/waveguide region grown on top of the three layers of coupled dots.

Light-current measurements under pulsed biasing was performed on 1.0μm p-doped TI QD lasers similar to the 1.3μm p-doped lasers described in the previous section. The results are summarized in Fig. 15(a) and (b). From the data of Fig. 15(b), T_0=205K can be extracted for p-doped tunnel injection lasers, which is relatively high but less than what observed in the 1.3μm p-doped SCH lasers. We believe the lower T_0 in the 1.0μm p-doped TI lasers is a consequence of the following: (a) As shown in Fig. 8(a), the Auger coefficients and their temperature dependence are smaller in TI lasers. Therefore, Auger recombination is unlikely to play the discussed dominant role to achieve high T_0; (b) recombination in the $In_{0.27}Ga_{0.83}As$ injector layer of the tunneling structure will reduce T_0.

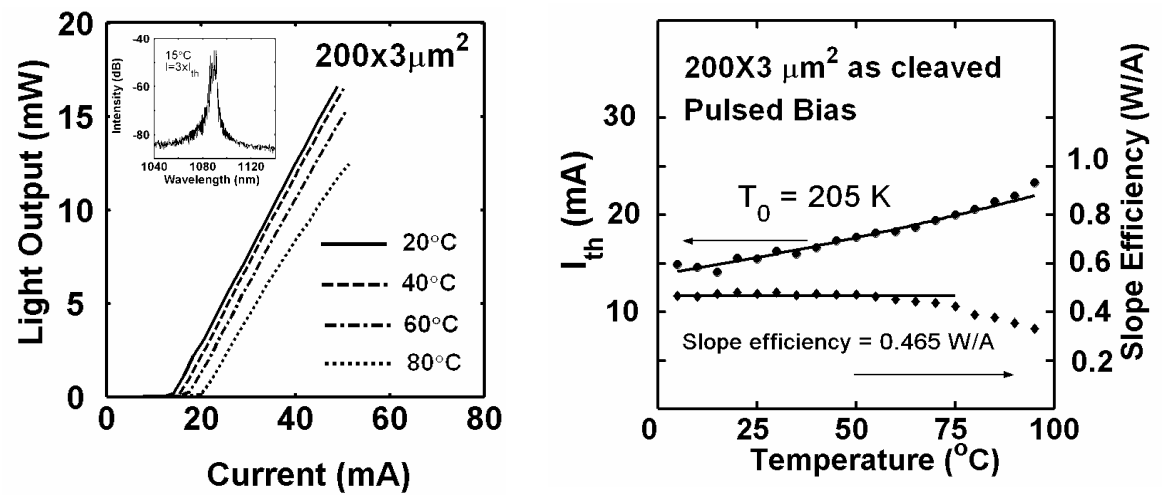

(a) (b)

Figure 15: (a) Pulsed light-current characteristics of 1.0μm p-doped tunnel injection single mode QD lasers at different temperatures. The inset shows the output spectrum at 15°C; (b) variation of threshold current and slope efficiency of the lasers with temperature. The lines are guides to the eye.

The small signal modulation response of 1.0μm p-doped TI QD lasers was measured with a high-speed photoreceiver, MITEQ low-noise amplifier and an electrical spectrum analyzer, after collecting the output light with a cleaved fiber. The measured small-signal modulation response was corrected by taking into account amplifier gain and loss in the microwave cables. The measurements were made under pulsed bias. The corrected modulation response for the lasers at room-temperature and at different injection currents is shown in Fig. 16(a). The maximum 3-dB bandwidth, measured for an injection bias of 100mA is ~24.5GHz, *which is the highest modulation bandwidth reported to date in quantum dot lasers.* The linewidth enhancement factor, α, of the tunnel injection lasers were measured at threshold by using the formula: $\alpha = \frac{2}{\partial\lambda} \frac{\Delta\lambda_i}{\Delta\{\ln[(\sqrt{r_i}-1)(\sqrt{r_i}+1)^{-1}]\}}$, where $\partial\lambda$ is the mode spacing, r_i is the peak-to-averaged valleys ratio of the *i*th competing mode in the optical spectrum, and ΔN is the incremental carrier density for two differential bias values. The sub-threshold spectra were measured under pulsed bias with a HP 70952B optical spectrum analyzer with a minimum resolution of 0.8Å at room temperature. It was observed that upon varying the voltage increment, ΔV, from differential value of 0.1V to values as high as 0.5V, no spectral differential shift of the longitudinal laser peaks, $\Delta\lambda_i$, was observed. Therefore, α~0 in the present p-doped tunnel injection laser within the resolution of our spectrum analyzer. This value is less than our previously reported α~0.7 for undoped TI QD lasers measured with the same setup.

Since chirp is directly proportional to α, tunnel injection QD lasers are expected to have ultra-low chirp. We measured the chirp in these devices from the difference of the linewidth of single longitudinal modes with and without superimposing an ac signal. The envelope of the dynamic shift in wavelength of the sinusoidal modulation signal was recorded with the optical spectrum analyzer. The measured chirp in TI-QD lasers as a function of modulating frequency, with a peak-to-peak modulation current of 22 mA and a dc bias of 72 mA, is shown in Fig. 16(b). As expected, the dynamic chirp is negligible (<0.4Å) and less than our previous values for undoped TI QD lasers.

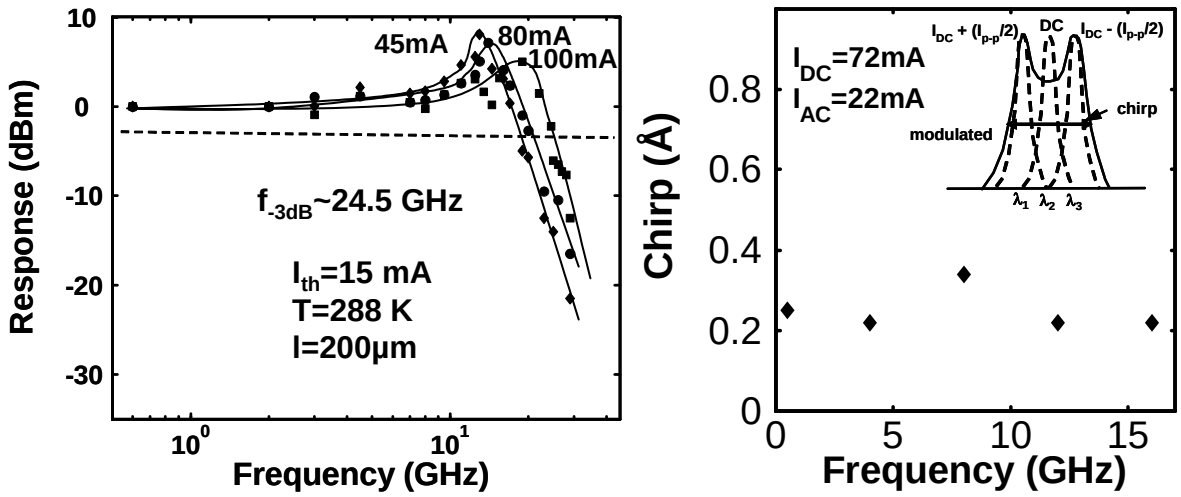

(a) (b)

Figure 16: (a) Modulation response of single-mode 1.0μm p-doped QD tunnel injection lasers at different biases at 15°C; (b) Measured chirp for the tunnel injection quantum dot lasers at different modulating frequencies at 15°C.

7. List of Publications and Conference Presentations:

[1] P. Bhattacharya, S. Fathpour, Z. Mi, and S. Chakrabarti, A. R. Kovsh, S. S. Mikhrin, I. L. Krestnikov, A. V. Kozhukhov, and N. N. Ledentsov (INVITED), "High Performance Quantum Dot Lasers", *UKC-Nano2004*, Research Triangle Park, NC, August 2004.

[2] S. Fathpour, Z. Mi, and P. Bhattacharya, A. R. Kovsh, S. S. Mikhrin, I. L. Krestnikov, A. V. Kozhukhov, and N. N. Ledentsov, "The Role of Auger Recombination in the Temperature Dependent Output Characteristics of p-Doped 1.3μm Quantum Dot Lasers", submitted to *Applied Physics Letters*, July 2004

[3] S. Fathpour, Z. Mi, S. Chakrabarti, P. Bhattacharya, A. R. Kovsh, S. S. Mikhrin, I. L. Krestnikov, A. V. Kozhukhov, and N. N. Ledentsov, "Characteristics of High-Performance 1.0 μm and 1.3 μm Quantum Dot Lasers: Impact of p-doping and Tunnel Injection" *62nd Device Research Conference Digest*, Notre Dame, IN, June 2004.

[4] S. Fathpour, P. Bhattacharya, and S. Ghosh, "Low linewidth enhancement factor and chirp and suppressed filamentation in tunnel injection $In_{0.4}Ga_{0.6}As$ self-assembled quantum dot lasers", *SPIE Photonics West,* San Jose, CA, January 2004.

[5] S. Fathpour, P. Bhattacharya, S. Pradhan, S. Ghosh, and J. Topolancik, "Modulation Characteristics of $In_{0.4}Ga_{0.6}As$/GaAs Quantum Dot Gain-Coupled Distributed Feedback Lasers", *IEEE Laser and Electro-Optics Society Meeting*, Tucson, AZ, November 2003.

[6] S. Fathpour, P. Bhattacharya, S. Pradhan, and S. Ghosh,"Linewidth Enhancement Factor and Near-Field Pattern in Tunnel Injection $In_{0.4}Ga_{0.6}As$ Self-Assembled Quantum Dot Lasers", *Electron. Lett.,* **39**, 1443 (2003).

[7] P. Bhattacharya**,** S. Ghosh, S. Pradhan, J. Singh, Z-K. Wu, and T. Norris, "Carrier dynamics and high-speed modulation properties of tunnel injection InGaAs/GaAs quantum dot lasers", *IEEE J. of Quantum Electron.*, **39**, 952 (2003).

[8] P. Bhattacharya (KEYNOTE), “High-Speed Quantum Dot Lasers”, *SPIE Photonics West*, San Jose, Ca, January 2003.
[9] P. Bhattacharya (INVITED), “High-Speed Quantum Dot Lasers and Quantum Dot Photinc Crystal Light Sources”, *Internatinal Symposium on Quantum Dots and Photonic Crystals*, Tokyo, Japan, Nivember 2003.
[10] S. Pradhan**,** S. Ghosh, and P. Bhattacharya, “Temperature dependent steady-state characteristics of high-performance tunnel injection InGaAs/GaAs quantum dot lasers”, *Electron. Lett.*, **38**, 1449 (2002).
[11] S. Ghosh, P. Bhattacharya, Z-K. Wu, T. Norris, J. Singh, and B. Kochman, "Quantum Dot Tunnel Injection Lasers with Large Modulation Bandwidth at Room Temperature", *Device Research Conference*, Santa Barbara, CA, June 2002.
[12] S. Pradhan, S. Ghosh, and P. Bhattacharya, "Modulation Characteristics of High-Speed Tunnel Injection In0.4Ga0.6As Quantum Dot Lasers", *IEEE Lasers and Electro-Optics Society Annual Meeting*, Glasgow, United Kingdom, November 2002.
[13] P. Bhattacharya and S. Ghosh, (INVITED) "High Speed Quantum Dot Lasers", *Conference on Optoelectronics and Microelectronic Materials and Devices* (COMMAD), Sidney, Australia, December 2002.
[14] S. Ghosh, P. Bhattacharya, E. Stones, J. Singh, H. Jiang, S. Nuttinck, and J. Laskar, “Temperature-dependent measurement of Auger recombination in self-organized $In_{0.4}Ga_{0.6}As$/GaAs quantum dots”, *Appl. Phys. Lett.* 79, 722 (2001).

8. Report of Inventions

None.

9. List of Scientific Personnel Supported, Degrees, Awards and Honors

Siddhartha Ghosh, GSRA
Sameer Pradhan, GSRA
Sasan Fathpour, GSRA
Zetian Mi, GSRA

Siddhartha Ghosh, Ph.D., “Growth of In(Ga)As/GaAs self-organized quantum dots and their application to high-speed lasers and spin-polarized light sources” (2003).

Sameer Pradhan, Ph.D., “Optoelectronic devices and integrated circuits for imaging applications” (2003).

Pallab Bhattacharya, Nick Holonyak, Jr. Award, Optical Society of America, 2002.

Pallab Bhattacharya, International Quantum Devices Award, International Symposium on Compound Semiconductors, 2003.

10. Technology Transition

None.